Construction and Building Materials 69 (2014) 60–72

Contents lists available at ScienceDirect

Construction and Building Materials

journal homepage: www.elsevier.com/locate/conbuildmat

Physico-chemical, mechanical, microstructure and durability characteristics of alkali activated Egyptian slag

Mohamed Heikal [a,b,*], M.Y. Nassar [a], G. El-Sayed [a], S.M. Ibrahim [a]

[a] Chemistry Department, Faculty of Science, Benha University, Benha, Egypt
[b] Chemistry Department, College of Science, Al Imam Mohammad Ibn Saud Islamic University (IMSIU), P.O. Box 90950, Riyadh 11623, Saudi Arabia

HIGHLIGHTS

- Alkali activator contents affected the location and intensities of the conductivity maximum.
- Mix S5 shows the higher values of compressive strength at all curing ages up to 90 days.
- Mix S1 shows higher values of strength in 5% $MgSO_4$ or $MgCl_2$ solution upto 180 days.
- Alkali activated GBFS improves the durability and the resistance to chemical attack.
- The total chloride and total sulphate contents decrease with alkali activated GBFS.

ARTICLE INFO

Article history:
Received 8 January 2014
Received in revised form 28 May 2014
Accepted 8 July 2014
Available online 7 August 2014

Keywords:
Alkaline activation
Electrical conductivity
Thermal analysis
Phase composition
Microstructure and durability

ABSTRACT

The aim of the present work is to study the characteristics of alkali activated Egyptian slag (GBFS) mixed with different contents of Na_2O and SiO_2. The rate of the kinetic of activation of GBFS has been studied by electrical conductivity, FTIR, DTA/TGA, XRD and SEM techniques. Electrical conductivity of alkali activated slag systems depends mainly on the binder composition, the activator type and its concentration. The increase in alkali activator contents affected the location and intensities of the conductivity maximum. As the hydration time increases the amount of hydration products increase, hence the chemically combined water and combined slag contents increase. SEM images showed the presence of (N,C)ASH gel with low porosity. With the increase of the content of Na_2O leads to form a denser closed microstructure, leading to higher compressive strength values. The activated GBFS showed good durability in 5% $MgSO_4$ or 5% $MgCl_2$ solution, i.e., the compressive strength increased gradually with immersing time up to 180 days. The total chloride and total sulphate contents decrease with alkali activated GBFS due to the forming hydrated products that fill some available open pores, thereby inhibiting Cl^- or SO_4^{2-} ions penetration; this effect leads to a decreased accessibility of Cl^- or SO_4^{2-} ions towards the more dense with low capillary pore structure. It can be concluded that alkali activated GBFS are more durable in 5% $MgSO_4$ or 5% $MgCl_2$ than OPC pastes.

1. Introduction

The role of alkali activated cements protect the environment through the utilization of by-product materials in their manufacture and end applications in waste management. The production of alkali-activated concretes is associated with low energy consumption and low CO_2 emission, along with the potential to reach high mechanical strength at early ages of curing, resistance to chemical attack and resistance to high thermally treated temperatures. These properties have made concretes based on alkali-activated binders a very interesting [1–3]. Portland cement (OPC) production increases global greenhouse gas emissions such as dioxin, NO_x, SO_2, and particulates, through the calcination of clinker in hydrocarbon heated furnaces. The high CO_2 emissions arising (7% of all CO_2 generated) from OPC manufacture have been attributed to calcination of limestone, which leads to formation and release of CO_2 and high energy consumption during manufacturing at temperatures up to 1550 °C [4]. Reduction in cement consumption has been attained by the use of industrial by products such as blast-furnace slag (GBFS), fly ash (FA), silica fume (SF) and cement kiln dust (CKD), as partial cement replacement materials [5,6].

* Corresponding author at: Chemistry Department, College of Science, Al Imam Mohammad Ibn Saud Islamic University (IMSIU), P.O. Box 90950, Riyadh 11623, Saudi Arabia. Tel.: +966 534484605; fax: +966 112591678.
E-mail address: ayaheikal@hotmail.com (M. Heikal).

http://dx.doi.org/10.1016/j.conbuildmat.2014.07.026
0950-0618/

Alkali activation is a process based on the action of solutions of alkali compounds like sodium or calcium hydroxide, sodium carbonate and silicate on the aluminosilicate constituent of the binder. The result is the destruction of the chemical bonds of the type Si—O—Si in the aluminosilicate. Alkali-activated binders (also referred as to 'geopolymers') are produced from an aluminosilicate source mixed with an alkaline solution [7]. These binders exhibit technological and ecological advantages in comparison with ordinary Portland cement (OPC), and the industrial use of geopolymer concretes in the production of high performance building materials is expanding [8]. A strong dependence on the nature of the alkaline activator in the structural and mechanical development of these binders has been identified throughout the literature. Alkali activated cements (AAC) are the type of the binders synthesized from natural alumino-silicate materials and aluminosilicate waste products such as fly ash, rice husk ash, and slag which are rich in silicium and aluminium [9]. Therefore, the use of alkali activation technology enables the possibility of substantial utilization of waste materials.

Development of geopolymers is the new, knowledge-based, multi-functional materials with higher performance, reduced environmental impact and adjustable to customer needs. Numerous studies have been conducted over the last few decades to determine the composition and microstructure property relationships in such systems [10–14]. Effect of workability, ultra fine materials, pore size distribution, early age strength, mechanical, cracking and shrinkage as well as the residual compressive strength behaviour of alkali activated slag paste (AASP) up to 1200 °C were investigated [15–22]. The workability, durability and strength are affected by the type and concentration of the alkaline activator, solution ratio (Ms = SiO_2/Na_2O), slag type, fineness, curing conditions, water/cement ratio, activating solution/slag ratio and the use of admixture as well as fibres [23–26]. Purdon [27] investigated the effect of NaOH concentration on strength of AAC. Glukhovsky et al. [28] classified alkaline activators into six groups according to their chemical compositions as a caustic alkalis, non-silicate weak acid salts, silicates, aluminates, aluminosilicates and non-silicate strong acid salts. NaOH, Na_2CO_3, $Na_2O{\cdot}nSiO_2$ and Na_2SO_4 are the most widely available and economical activators. The factors affecting on the strength of alkali activated GBFS were the type, and the dosage of alkali as well as the type and fineness of slag, SiO_2/Na_2O ratio, curing temperature, water/slag ratio and additive as well as [29,30].

The effectiveness of the alkali activator is a very significant factor influencing the intensity and rate of process of alkali activation. It is reported that the best activator is waterglass [31,32]. The best dosage is within the range of 3.0–5.5% Na_2O by of slag. The optimum dosage ranges of waterglass solution are 0.75–1.25% for acid GBFS, 0.90–1.30% for neutral GBFS and 1.0–1.5% for basic GBFS. The optimum range of fineness is 4000–5500 cm^2/g. It is evident that the effectiveness of activator is a very significant factor which determines the engineering properties of the material. Sodium silicate (SSL) has been extensively used in the activation of aluminosilicate precursors such as GBFS, metakaolin (MK), FA and others [23,33].

The sulphate and chloride ions can enter into deleterious reactions leading to the dissolution of CH, precipitation of gypsum and sulfoaluminates as well as Friedel's salt, which cause expansion and softening of concrete, respectively [34,35]. The presence of Mg^{2+} as $MgSO_4$ and/or $MgCl_2$ leads to the distortion of C—S—H through a dissolution of Ca^{2+} and/or an exchange with Mg^{2+} to give also Mg—S—H and CH. All the above mentioned reactions are accompanied by decrease in strength [36–40]. El-Didamony et al. [41] represented the experimental trials to activate GBFS to produce cementless binding materials. The results revealed that the increase of NaOH content increase the chemically combined water contents up to 90 days. On the other hand, the bulk density and compressive strength were increased by increasing Na_2SiO_3 content in presence of NaOH. The increase of compressive strength is due the increase of $[SiO_4]^{4-}$ which enhances the C—S—H formation. The durability of alkali activated GBFS mortars and concretes have been studied. Alkali activated GBFS are durable binder in sulphate, sea water and acid resistant [42–48]. Darko and Branislav [49] examined the early hydration of alkali–GBFS metasilicate ($Na_2SiO_3{\cdot}5H_2O$) solution at 25 °C. The compressive strength of AAC is higher than OPC mortar. The feasibility of using an alkaline activated GBFS to produce a mortar without using OPC was investigated [50].

The reaction mechanism of aluminosilicates containing a calcium bearing compound differs from the geopolymeric reaction as explained. It has also been reported that the type of calcium bearing compound in the starting material play an important role in the alkali activation of these materials. Alkalis first attack the GBFS particles breaking the outer layer and then a polycondensation of reaction products takes place. Wang et al. [51] suggested that the initial reaction products formed by the dissolution and precipitation, whereas, at later ages, a solid state mechanism is followed where the reaction takes place on the surface of the formed particles, dominated by slow diffusion of the ionic species into the unreacted core. Alkali cation (R^+) acts as a mere catalyst for the reaction in the initial stages of hydration, via cation exchange with the Ca^{2+} ions [52,53]. The alkaline cations act as structure creators. The nature of the anion in the solution also plays a determining role in activation, particularly in early ages and especially with regard to paste setting [47,54]. The final products of the GBFS reaction are similar to the products of cement hydration (C—S—H); the major difference being the rate and intensity of the reaction. It has also been observed that the alkalis are bound to the reaction products and are not freely available in the pore solution (this depends on the alkali concentration used, though), thereby a small percentage of the alkalis (around 0.02%) are bound to the reaction products but most of the alkalis remains in the pore solution [55].

This paper studied the influence of different alkaline concentrations on the hydration characteristics and morphology of GBFS system. These characteristics were investigated by changing the initial alkalinity of the hydration condition in order to reveal the affecting mechanism of alkaline condition on its hydration.

2. Experimental techniques

2.1. Materials

Egyptian blast-furnace slag (GBFS) was provided from Iron and Steel Company, Helwan Governorate, Egypt. Its chemical oxide composition is given in Table 1. XRD patterns, FTIR spectra and SEM are shown in Figs. 1–3. Blaine surface area of slag was 4500 ± 50 cm^2/g. The diffraction patterns of GBFS was shown in Fig. 1. The diffractogram of the unreacted slag shows a predominantly amorphous material. There is also a broad feature 'amorphous hump' between 20 and 38° 2θ attributed to the amorphous glassy component.

Table 1
Chemical composition of starting materials, mass %.

Oxide composition (%)	GBFS	OPC	SSL
SiO_2	37.81	21.40	30.7
Al_2O_3	13.14	3.67	–
Fe_2O_3	0.23	5.05	–
CaO	38.70	64.03	–
MgO	7.11	1.50	–
SO_3	1.19	2.05	–
Na_2O	1.03	0.30	10.3
K_2O	0.19	0.22	–
TiO_2	0.34		–
P_2O_5	0.16		–
L.O.I.	0.00	1.60	59.0
Total	99.90	99.82	100.0

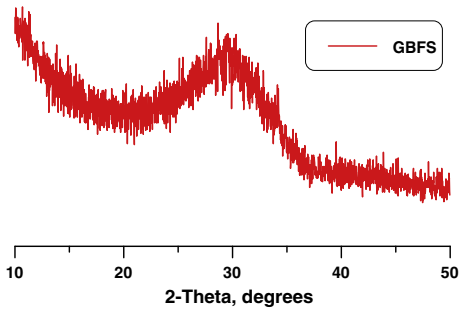

Fig. 1. XRD pattern of GBFS.

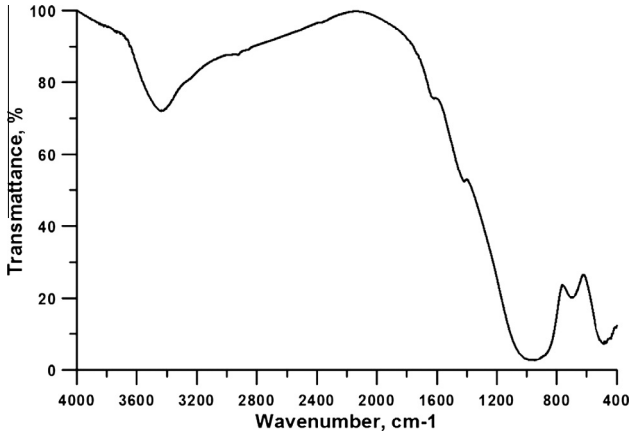

Fig. 2. FTIR spectra of GBFS.

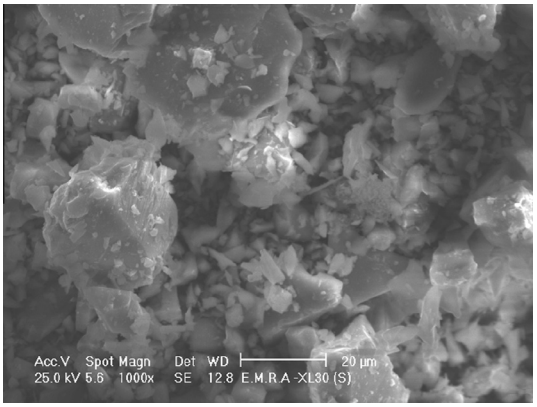

Fig. 3. SEM of GBFS.

Fig. 2 represents FTIR spectra of GBFS. It contains two main bands at 484.93 and 967 cm^{-1} as well as two bands less intense at 697.79 and 1422 cm^{-1}. Bands at 967 and 484.93 cm^{-1} imply the presence of orthosilicate units $[Si_2O_7]^{6-}$ with partial substitution of Si^{4+} by Al^{3+} in tetrahedral positions. These units are built of two silicooxygen (or silico/and aluminooxygen) tetrahedra, connected with oxygen bridge. The two bands at 967 and 484.93 cm^{-1} represent the internal vibrations of $[SiO_4]^{4-}$ and $[AlO_4]^{5-}$ tetrahedral. The first comes from Si(Al)—O asymmetric stretching vibrations; the second should be assigned to O—Si—O bonds bending vibration. The appearance of the most intense band at relatively low wave numbers proves that, the silicate phases occurring in the GBFS containing orthosilicate units $[Si_2O_7]^{6-}$. The existence of the weak band at 697.79 cm^{-1}, assigned to the symmetric stretching vibrations of the Si—O—Si(Al) bridges, further confirms the presence of these units. It is possible to suppose that, it is also connected with vibrations of Si—O—Al bridges, formed by linkage of $[SiO_4]^{4-}$ and $[AlO_4]^{5-}$ tetrahedral. The broadness of the band located at 967 cm^{-1} proves the significant content of glassy phase in the structure of GBFS. GBFS particle morphologies obtained using SEM is shown in Fig. 3. GBFS is composed of angular particles of varying sizes. This material presents a mean particle size of about 12 µm and irregular shape morphology with a dense-compact structure.

NaOH was produced by SHIDO Company with purity 99%, commercial sodium silicate liquid (SSL) was provided from Islamic Silicate Industry, Badr City, Helwan. Sodium silicate liquid consists of 30.7% SiO_2, 10.3% Na_2O and 59% H_2O with silica modulus SiO_2/Na_2O equal 2.98 and density 1.44 g/cm^3 was used. Sodium silicate solutions were used as activators and caustic soda content was increased by the addition of sodium hydroxide (NaOH) pellets.

GBFS was firstly crushed in a jaw crusher to pass through a 2 mm diameter sieve, then passed through a magnetic separator to remove any contamination of iron melt then ground in steel ball mill to reach 4500 ± 50 cm^2/g Blaine surface area. Different mixes were prepared from GBFS using mixed activators as shown in Table 2. The pastes were prepared using NaOH (SH) and sodium silicate liquid Na_2SiO_3 (SSL) as activators as shown in Table 2. The resulting solution was then allowed to cool down to the room temperature for about 2 h. GBFS was mixed with tap water. The water to binder ratio (w/b) is 0.30 [56].

The mix compositions were prepared as shown in Table 2. The ingredients of each mix were blended in a porcelain ball mill for 1 h using a mechanical roller mill to ensure complete homogeneity. GBFS was placed on smooth, non-absorbent surface, a crater was formed in the centre and the mixing water with the activator was poured into the crater as shown in Table 2. The mixing process was performed according to ASTM specification [56]. The mixture was slightly troweled to absorb the water for about 1 min, and then completed by vigorous mixing for 3 min. The pastes were moulded in one inch cubic moulds, then strong manually pressed into the moulds. The surface of the paste was then smoothed by thin edged trowel. Immediately after moulding, the specimens were cured in 100% RH at 35 °C for 24 h, then demoulded and cured in the humidifier up to 3 days, then cured under tap water after 3 days up to 90 days. For the specimens which were tested for the resistivity against 5% magnesium sulphate and magnesium chloride attack, the specimens were cured up to 7 days (zero time) in tap water then immersed in the aggressive solution 5% $MgSO_4$ or $MgCl_2$ up to 180 days. The aggressive solution was renewed monthly to maintain constant concentration.

In electrical conductivity measurements the test cell was of the co-axial type and included concentric inner and outer electrodes mounted on an insulated base plate as shown in Fig. 4. The electrodes were polished before the experiment [57,58]. The mixing was done with the required amount of water that gives normal consistency in the presence of suitable amount of alkaline activator (SiO_2/Na_2O mol/kg). The measurements of the electrical conductivity were begun exactly 3 min after mixing with water (0 time). The pastes were placed in the space between the electrodes. The cell was kept in a cabinet chamber at 100% relative humidity during the test period from 3 min up to 28 days. The electrical conductivity was measured at 35 °C. The electrodes were connected with RLC meter, model SR-720. All data of the electrical conductivity were measured during the setting and hardening at relativity low AC frequency 1V and 1000 Hz for resistance measurements.

Table 2
Composition of the investigated mixes containing alkaline activator ($SiO_2 + Na_2O$), mixing with 1 kg of GBFS.

Mix no.	SiO_2 (mol/kg of GBFS)	Na_2O (mol/kg of GBFS)	H_2O (mL/kg of GBFS)
S1	0.50	0.25	300
S2	0.50	0.50	300
S3	0.50	0.75	300
S4	0.50	1.00	300
S5	0.50	1.25	300
S6	0.50	1.50	300
OPC	–	–	270

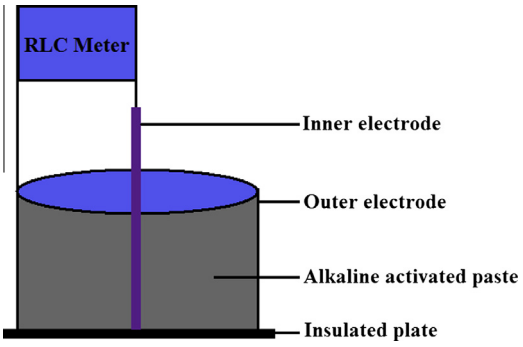

Fig. 4. Electrical conductivity cell.

The compressive strength was done on a compression machine of SEIDNER, Riedinger, Germany, with maximum capacity of 600 kN force. The compressive strength was carried out on four samples as described by ASTM Specifications (ASTM Designation: C-150, 2007). The bulk density was carried out before the pastes subjected to compressive strength determination through weighing the hardened pastes (suspended in water) and in air (saturated surface dry). Each measurement was conducted on at least three similar cubes of the same age [38]. After, the determination of bulk density, four cubes of the same age were dried in a furnace at 105 °C for 24 h then weighed after cooling in a desiccator. The total porosity of the cement pastes could be calculated [38].

The hydration of cement pastes were stopped by pulverizing 10 g of representative sample in a beaker containing methanol–acetone mixture (1:1), then mechanically stirred for 1 h. The mixture was filtered through a gooch crucible, G_4 and washed several times with the stopping solution then with ether. The solid was dried at 70 °C for 1-h complete evaporation of alcohol then collected in polyethylene bags; sealed and stored in desiccators for analysis [38]. The combined water content (W_n) considered as the percent of ignition loss of the dried samples (on the ignited weight basis). Approximately 2 g of the predried sample were gradually ignited up to 800 °C for 1 h soaking time [38].

Anhydrous slag content determined according to the methods reported in earlier publication [59]. 1 g sample is treated with 5 g salicylic acid, 70 ml acetone and 30 ml methanol. After the mixture has been stirred (1 h, magnetic stirrer), the resulting solution is stored for 24 h in an airtight container. The solution is then filtered on a G_4 glass filter and the filter residue is washed with 200 ml methanol. The residue obtained is dried at 45 °C for 24 h, and then heated at 800 °C for 20 min in an electrical furnace. These burning conditions are selected so that oxidation of slag constituents is largely avoided. The residue from the solution is weighed after the crucible has been cooled in desiccator. Corrections were made for neat slag and the loss of ignition at 800 °C [60].

Thermal gravimetric analysis (TGA) was carried out using DTA-50 Thermal Analyzer (Schimadzu Co., Tokyo, Japan). A dried sample of about 50 mg (−53 μm) was used at heating rate 20 °C/min under nitrogen atmosphere. For IR spectroscopic investigation, the samples were prepared using alkali halide KBr pressed disk technique. The IR analysis was recorded from KBr disks using Gensis FT-IR spectrometer in the range 400–4000 cm^{-1} after 256 scans at 2 cm^{-1} resolution.

The scanning electron microscope (SEM) was taken with Inspect S (FEI Company, Holland) equipped with an energy dispersive X-ray analyzer (EDX). SEM was used to examine the microstructure of the fractured composites at the accelerating voltage of 200–30 kV and power zoom magnification up to 300,000×. The samples are firstly dried at 70 °C until constant weight, then, bonded on the sample holders with conducting glue carbon. The morphologies of the products are observed at microscopic level.

The total sulphate content was gravimetrically estimated by using 1 g sample dissolved in 5 m1 of concentrated HCl and 100 ml of distilled water were added, then boil for 5 min, filter and wash several times with distilled water. Add to the filtrate 10 ml of 10% $BaCl_2$, digest, filter and ignite at 1000 °C for 30 min. The total sulphate content was calculated as:

$$SO_3\% = \frac{\text{weight of ppt}}{M} \times 34.3$$

where M is the weight of sample in grams [38].

Total chloride was determined by weight 2 g into a stopper conical flask, dispersed with 25 ml water and then added 10 ml of nitric acid (sp. gr. 1.42). Add 50 ml hot water, heat to near boiling and keep warm for 10–15 min. If the supernatant liquid is turbid, filter through filter paper (41) and wash with hot water, then cool to room temperature. An excess of standard 0.1 N $AgNO_3$ was added and 2–3 ml of nitrobenzene to coagulate the precipitate, stopple the flask and shake vigorously, then add 1 ml of ammonium ferric alum as indicator and titrate against standard 0.1 N ammonium thiocyanate [38].

3. Results and discussion

3.1. Electrical conductivity

The variations of electrical conductivity were studied with the increase of the hydration time [58,61,62]. Electrical conductivity of alkali activated GBFS with different content of Na_2O from 0.25 to 1.5 mol with 0.50 mol of SiO_2 was given in Fig. 5. The increasing of the alkalinity condition can promote the hydration of alkali activated GBFS, which increases the degree of hydrolytic destruction of the GBFS. The addition of alkali cations into the activating solution have two effects; first, it increases the pH in the solution; (higher amounts of OH^- ions) that helps to sever the Si—O—Si and Si—O—Al bonds of the alkali activated GBFS into silicate and aluminate species [7]; second, the alkali cation balances the electric charge in the tetrahedral Si and Al structure [63].

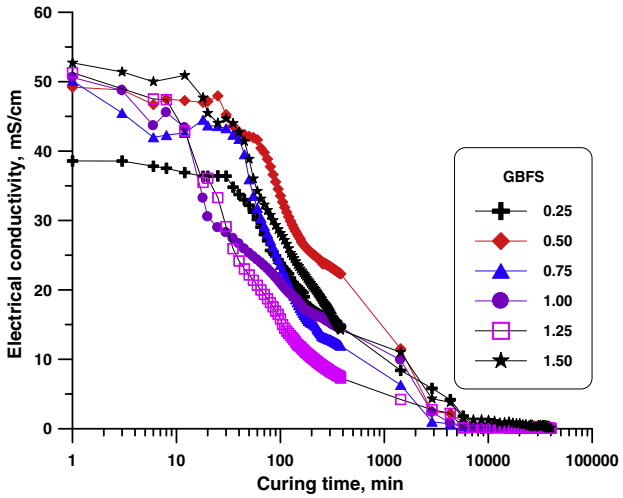

Fig. 5. Electrical conductivity of alkali activated GBFS with different contents of Na_2O and/or 0.50 mol SiO_2 cured up to 90 days.

Electrical conductivity of alkali activated GBFS systems depends mainly on the binder composition, the activator type and its concentration. Fig. 5 showed that the initial electrical conductivity increases with the Na_2O content increases, free OH^- and Na^+ ions were released from the pores of the fresh paste (the initial stage – predormant period). After 20–30 min the results showed a decrease in the electrical conductivity values, indicating the geopolymerization reaction progress by the consumption of OH^- and Na^+ ions. Mix S1 (0.25:0.50; Na_2O:SiO_2 mol/kg of GBFS) shows the lowest value of initial electrical conductivity. The increase of the alkali activator contents, the initial electrical conductivity increases as shown for mixes S2, S3, S4, S5, and S6 (0.50–1.50:0.50; Na_2O:SiO_2 mol/kg of GBFS).

As the concentration of alkali activator increases, very high ionic association starts taking place, then the concentration of ions start decreasing (initial rapid reaction period). Evidently, the conductance–time curves show one conductivity maximum followed by a sharp decrease in the conductivity value. The decrease in the conductivity values is mainly attributed to the formation of electrically insulating layers around the alkali activated GBFS particles and/or the decrease in the number of ions as a result of the formation of hydration products. A very thin layer consisting of low Ca/Si ratio C—S—H, C—A—H and C—A—S—H, which has a very low solubility, precipitates very quickly through the solution, this can be observed after 20–30 min [64]. The increase in alkali activator contents affected the location and intensities of the conductivity maximum. Conductance increases with alkali activator contents due to the high content of free OH^- and Na^+ ions. This effect leads to an increase in the intensity of the conductivity maximum, which is also shifted to a short time. With the increase in the amount of alkali activator contents to reach 1.50 Na_2O mol/kg of GBFS, the conductivity maximum increases. The activation of GBFS proceeds via two steps. The first step is the pre-induction period (wetting and the slag particles start to dissolve). As the hydration proceeds, OH^- in the solution can break Ca—O, Si—O and Al—O bonds. These dissolved species exist in water in the form of $(H_2SiO_4)^{2-}$, $(H_3SiO_4)^-$, $(H_4AlO_4)^-$ and Ca^{2+} as a result of this the electrical conductivity increases, this period is called the induction period. After this period the a layer consisting of low Ca/Si ratio C—S—H, C—A—H and C—A—S—H precipitated very quickly through the solution [64]. Increasing the curing age permits more accumulation of hydration products that confirm the decrease in electrical conductivity. Alkali

activated GBFS pastes activated with $Na_2O:SiO_2$ after 28 days of reaction presented the formation of large amounts of amorphous C—S—H, C—A—H and C—A—S—H gel (geopolymer) [65,66].

3.2. Chemically combined water contents

Chemically combined water (W_n) contents of alkali activated GBFS cured up to 90 days are graphically represented in Fig. 6. The W_n content can be adopted as a criterion to evaluate the relative amount of hydration products and the relative hydration degree between different samples with the same kind of hydration products. It is clear that the combined water contents of the alkali activated GBFS pastes gradually increases up to 90 days. This is due to the continuous hydration and accumulation of hydrated products, which deposed in the available open pores. Fig. 6 shows the W_n contents of the 6 samples at the ages of 3, 7, 28 and 90 days. The increase of the hydration age, the W_n content of alkali activated GBFS increases with increases the contents of Na_2O from 0.25 to 1.5 mol/kg of GBFS in the presence of 0.50 mol of SiO_2/kg of GBFS. The increasing of the alkalinity condition can promote the hydration of alkali activated GBFS, which increases the degree of hydrolytic destruction of the GBFS. The W_n content of mix S1 at the age of 3 days is 2.98%, but those of mix S6 at the same age reaches 6.07%, indicating that the degree of hydrolytic destruction of alkali activated GBFS increases with the content of Na_2O.

Fig. 6 indicates that the influence of increasing alkalinity of hydration condition on the hydration of GBFS changes with age. Increasing alkalinity of hydration condition has an obvious promoting effect on the hydration of GBFS within 7–28 days. At the age of 90 days, the W_n contents of mixes S1, S2, S3, S4, S5, and S6 were 9.38%, 10.32%, 10.99%, 11.01%, 12.46% and 12.63% respectively. As the hydration time increases the amount of hydration products increase, hence the chemically combined water content increases, this is mainly due to the higher hydraulic properties of GBFS with the increasing of alkaline concentration.

3.3. Combined slag contents

The results of combined slag contents of alkali activated GBFS pastes are graphically plotted as a function of curing time up to 90 days in Fig. 7. The combined slag content increases with curing time due to the activation of GBFS hydration. C—S—H gel and C—A—S—H hydrated products are responsible for the strength increase in matrices containing GBFS. The formation of C—S—H and C—A—S—H within the binder work as a micro-aggregate, the

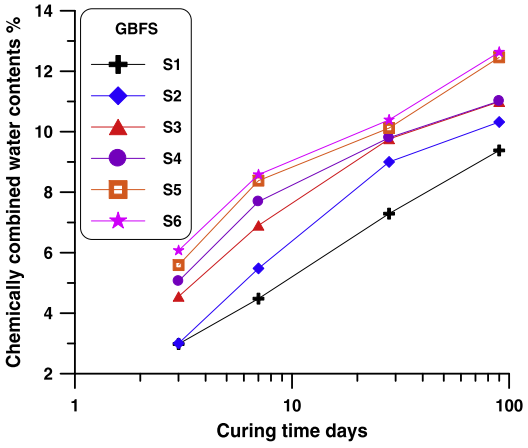

Fig. 6. Chemically combined water contents of activated GBFS as a function of curing time up to 90 days.

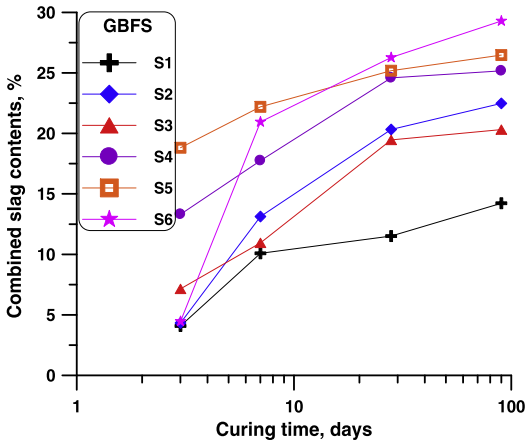

Fig. 7. Combined slag contents of activated GBFS as a function of curing time up to 90 days.

resultant binder is homogeneous and dense, resulting in increased mechanical strength as shown later [67]. The activation of GBFS with $Na_2O:SiO_2$ depends on the concentration of OH^- ions, the compositions of the layers (the concentration of —Si—OH and ≡Al—OH groups) and the solution. At higher concentration of OH^- ions the silicate and aluminate species get into the solution as hydroxocomplexes-silicate and aluminate anions, mostly condensed. The slag disintegration mechanism proceeded with regard to the types of oxygen O^{2-} present in GBFS. Three types of oxygen anion: double-fixed (siloxane bond ≡Si—O—Si≡), single-fixed (≡Si—O—Me— bond) and free in (—Me—O—Me— bond), where Me is a divalent cation. The reaction in aqueous medium may proceed according to the following equations:

$$\equiv Si—O—Si\equiv + H_2O \rightarrow 2\equiv Si—OH$$

$$\equiv Si—O—Me—O—Si\equiv + H_2O \rightarrow 2\equiv Si—OH + Me^{2+} + OH^-$$

$$\equiv Si—O—Me—O—Me—O—Si\equiv + 3H_2O \rightarrow 2\equiv Si—OH + 2Me^{2+} + 4OH^-$$

The surface silanol groups are neutralized in alkaline media, they act as a cation exchanger.

$$\equiv Si—OH + NaOH \rightarrow \equiv Si—O—Na + H_2O$$

Alumina is present in a similar formation, giving rise to soluble aluminate anion $Al(OH)^{4-}$ hydroxocomoles and surface groups, ≡Al—OH. As seen in the above equations, the equilibrium between the solid phase and aqueous solution depends on the concentration of OH-ions. The siliceous species could exist in the form of $[(HO)_2SiO_2]^{2-}$ and $[HOSiO_3]^{3-}$ under highly alkaline conditions [66]. C—S—H is generated by the reaction of Ca^{2+}, $HOSiO_3^{3-}$ and OH^- ions:

$$Ca^{2+} + HOSiO_3^{3-} + OH^- \rightarrow CaSiO_4H_2O$$

C—S—H is primarily responsible for the strength [68]. Jiaying and Peinan [69] showed that the GBFS has hardly any activity in water, while in alkali hydration and hardening are pronounced. The Si—O layer of the GBFS structure is destroyed by an alkali activator and hydration products, such as C—S—H gel and hydrocalcium aluminate are formed by rearrangement of SiO_4^{4-} and AlO_4^{5-} and produced gehlenite like hydrate (C_2ASH_8). GBFS–cement reacts with water, producing calcium aluminosilicate (C_2ASH_8), calcium aluminate, C_4AH_{13} hydrates and $Ca(OH)_2$, those products have the same properties as in the hydration of

pure Portland cement. In the alkali $Ca(OH)_2$ solution, Ca^{2+}, AlO_4^{5-}, and SiO_4^{4-} ions enter into the solution and form new hydrate (such as the hydrated silicate and the hydrated aluminate). Combined slag content increases as the concentration of alkali activated mixture. The increase of Na_2O contents from 0.25 mol to 1.50 mol in the presence of 0.50 mol of SiO_2 tends to increase the hydration of alkali activated GBFS at later ages of hydration (90 days). This can be seen from the gradual increase of combined slag contents after 90 days of hydration age.

3.4. Compressive strength

The compressive strength of hardened alkali activated GBFS cured up to 90 days. These values are graphically represented in Fig. 8. The compressive strength of all mixes increases with curing time. Mix S5 shows the higher values of compressive strength at all curing ages of hydration. As the amount of alkali activator increases, the compressive strength enhances. From the data represented in Fig. 8 it is clear that the values of the compressive strength increase is due to the higher rate of hydration as well as formation of more hydrated products. Compressive strength of mixes S3, S4, S5 and S6 sharply increases from 7 up to 90 days due to its reactivity at later ages. The compressive strength of hardened activated GBFS increases by the alkali contents, which accelerate the activation process. Further increase in Na_2O content (till 1.25–1.5 mol/kg) was reported to result in a decrease of compressive strength [34]. One plausible reason is that increasing of Na_2O content contents in activating solution may resulted in reduced level of long-range structural ordering products [10]. The compressive strength is in a good agreement with TGA/DTA analysis. The improvement on compressive strength is related to the reorganization in the microstructure of alkali activated GBFS system.

3.5. Bulk density

The bulk density of hardened activated GBFS cured up to 90 days is graphically plotted in Fig. 9. It is clear that the bulk density increases with curing time up to 90 days. The bulk density of alkali activated GBFS increases with curing time due to the continuous activation and formation of hydrated products. These hydrated products are deposited in the open pores that increase the bulk density of the activated slag. The increase of alkali activator enhances the bulk density of the investigated pastes. The alkali activator enhances the production of higher concentration of $[SiO_4]^{-4}$ which increases the rate of hydration and formation of more C—S—H and C—A—S—H. As the amount alkali activator content increases (X Na_2O mol/kg), the bulk density accordingly

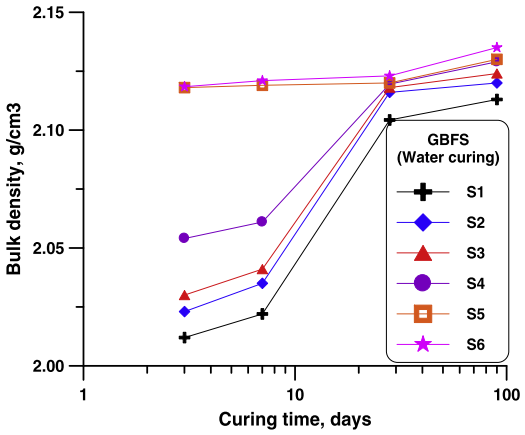

Fig. 9. Bulk density of activated GBFS and cured up to 90 days.

increases; this is mainly due to the high formation of hydrated products have high specific gravity.

3.6. Total porosity

The total porosity for alkaline activated GBFS is graphically plotted as a function of curing time Fig. 10. As the alkaline activation of GBFS increases, more hydration products are formed, which precipitated in some available open pores leading to decrease the total porosity. The addition of 1.25 mol of Na_2O (mix S5) gives the lower values of total porosity. The sharp decrease in the total porosity values of mixes S3 and S4 was shown up to 90 days of hydration. On the other side, the decrease in the total porosity values occurred after 28 days for mix S5 and S6. This is mainly due to the increase of the content of alkaline activator, which accelerates the activation of GBFS forming more hydration products. These hydration products fill a part of the available pore volume of the paste; therefore the total porosity decreases.

3.7. Thermo-gravimetric analysis

Figs. 11–13 present TGA/DTA thermograms of alkaline activated mixes S1, S3 and S6 cured for 3, 7 and 90 days. The weight loss of mix S1 at 1000 °C was found to be 3.88%, 8.93% and 10.48%, where for mix S3 was 5.24%, 9.77% and 10.94%, as well as for mix S6 was 6.57%, 10.36% and 11.76% at 3, 28 and 90 days, respectively. The increase in weight loss is related to the progress of geopolymerization process. The weight loss observed in TGA for geopolymerized paste is attributed to the decomposition (water loss) of these

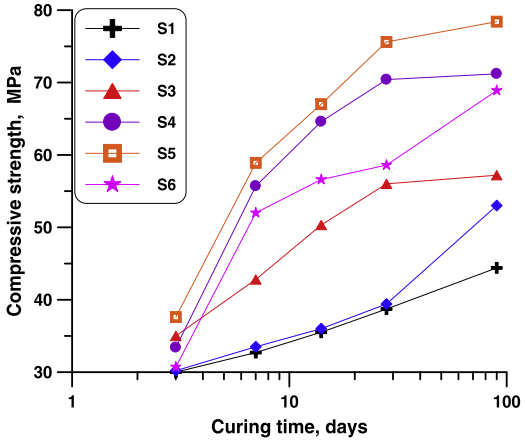

Fig. 8. Compressive strength of activated GBFS as a function of curing time up to 90 days.

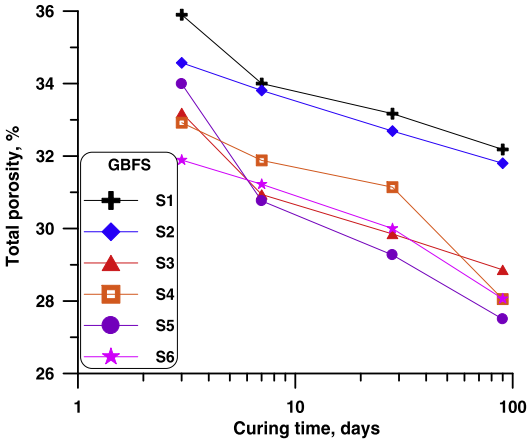

Fig. 10. Total porosity of alkali activated GBFS and cured up to 90 days.

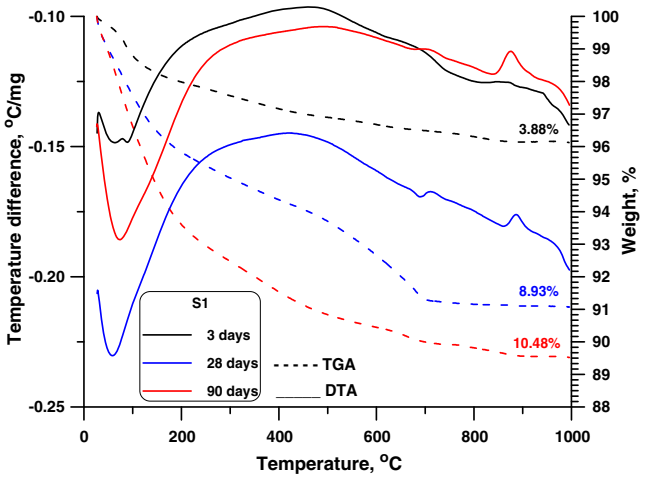

Fig. 11. DTA/TG thermograms of mix S1 activated with (0.25:0.50; Na_2O:SiO_2 mol/kg) cured up to 90 days.

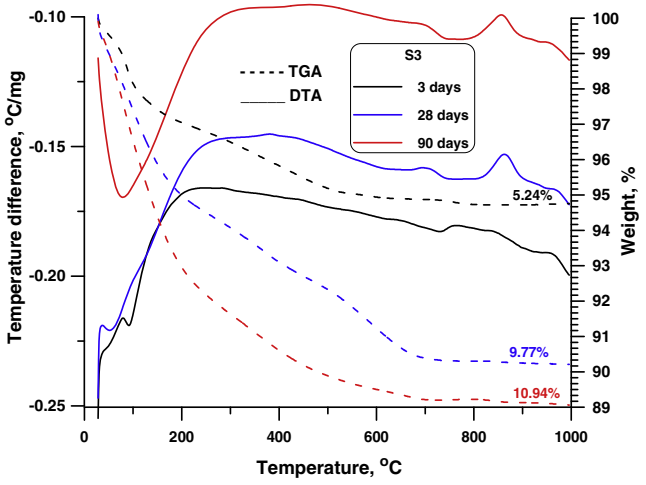

Fig. 12. DTA/TG thermograms of mix S3 activated with (0.75:0.50; Na_2O:SiO_2 mol/kg) cured up to 90 days.

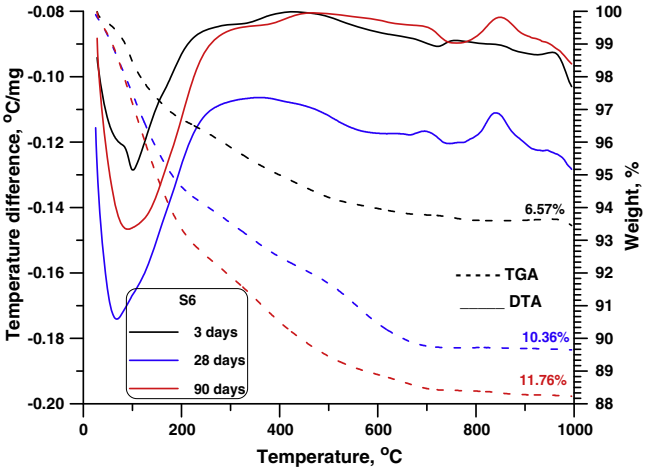

Fig. 13. DTA/TG thermograms of mix S6 activated with (1.50:0.50; Na_2O:SiO_2 mol/kg) cured up to 90 days.

Si—OH groups and Al—OH groups. The endothermic peak located at 60–101.75 °C is due to the dehydration of free water and C—S—H from hydrated matrix. The endothermic peaks located below 200 °C related to C—A—S—H and C—A—H as well as and the peak located at 260–360 °C due to the decomposition of C_4AH_{13} and C—A—H and C—A—S—H [70]. The endothermic peak located at 650–720 °C related to the decomposition of carbonate.

The weight loss due to the dehydration of interlayer water of C—S—H of mix S1 was 2.224%, 4.017% and 6.004%, where for mix S3 was 2.824%, 4.817% and 6.684%, as well as for mix S6 was 4.409%, 5.437% and 7.114% for the pastes cured after 3, 28 and 90 days, respectively. A general increase in weight loss with curing time is observed, which may be associated with a greater degree of alkaline activation [71]. The weight loss generally increases with Na^+ concentration, can be related to a higher degree of chemically bounded water and OH^- groups, provided alkaline activation, in the binding phase. The exothermic peak located at 850–870 °C is attributed to the crystallization of the pseudo-wollastonite phase (monocalcium silicate, CS). This exothermic peak is characteristic for the decomposition of C—S—H [72].

The main features of thermograms are characterized by an increase in the areas and intensities of the peaks located at 60 and 101.75 °C, which is due to the dehydration of free water and interlayer water of C—S—H, the peak area and its crystallinity increase of with curing time. As shown from TGA/DTA thermograms an increase in the areas and intensities of the peaks characteristic for C—S—H with the pH value of initial hydration condition (increases the contents of Na_2O) and age of the hydration up to 90 days. As the curing time increases the exothermic peak located at 850–870 °C shows an increase in the areas and intensities of the crystallization of the pseudo-wollastonite phase.

Thermogravimetric data for alkali-activated GBFS paste using different contents of Na_2O and sodium silicate are shown in Figs. 11–13. These tend to have a broader first peak located at (60–100.75 °C) when the amount of Na_2O is increased. The second peak (280–360 °C) can be clearly distinguished for 1.50 mol/kg of Na_2O (Fig. 13), and it progressively overlaps with the first peak when the concentration of the solution is increased, this is because zeolitic-like phases are less likely to form in highly concentrated solutions due to increased difficulties in phase transport and reorganization.

3.8. X-ray diffraction

Figs. 14–16, presented the XRD patterns of alkali-activated GBFS samples. It can be observed that the hump peak in the range of 20–38° 2θ changes in the period of curing time at 1 day to 90 days, suggesting that poor crystalline C—S—H and C—A—S—H gel produced in the pastes [73]. Indeed, once GBFS powder is mixed with the alkaline solution, geopolymer gel and C—S—H gel could be formed after setting and hardening. The geopolymer exhibits increase in the mechanical properties as shown in Fig. 8. For all XRD diagrams, broad and diffuse peaks are shown around d = 2.96–3.03 Å, implying amorphous or short-ordering structure phases generally present in alkali-activated GBFS. In alkali-activated GBFS, regardless of the presence of the strong peak at d = 3.07 Å is attributed to C—S—H(I) phases, which are composed of synthetic calcium silicate hydrate type (I). The formation of CSH or C—S—H(I) in alkali-activated slag has been reported in the literatures [47,73].

The hydrotalcite phase was also synthesized in both of the alkali-activated GBFS samples (d = 7.77–7.79, 3.85–3.87, 3.85, 2.58, 2.28–2.29, 1.98 Å). Several previous studies have reported that a hydrotalcite phase forms in alkali-activated GBFS pastes and pointed out that this phase is also a major phase of alkali-activated slag together with CSH(I) [73]. It is note that new phases, tobermolite and calcium silicate hydrate (CSH) gel, are generated during curing time of 28–90 days.

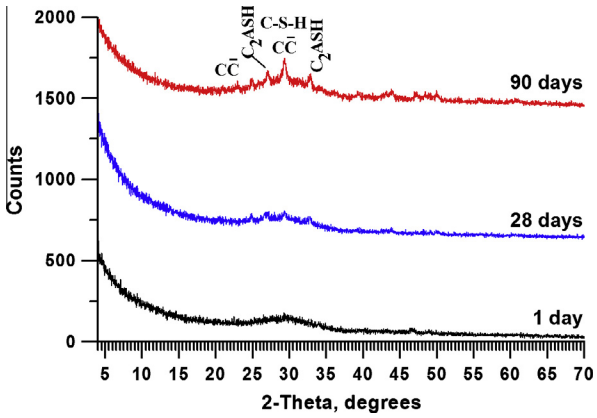

Fig. 14. XRD pattrens of mix S1 activated with (0.25:0.50; Na_2O:SiO_2 mol/kg) cured up to 90 days.

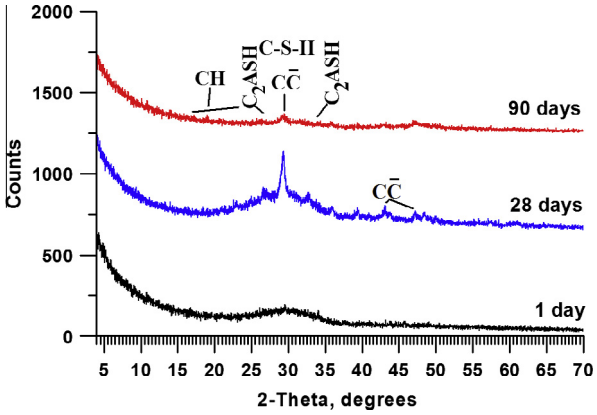

Fig. 15. XRD pattrens of mix S3 activated with (0.75:0.50; Na_2O:SiO_2 mol/kg) cured up to 90 days.

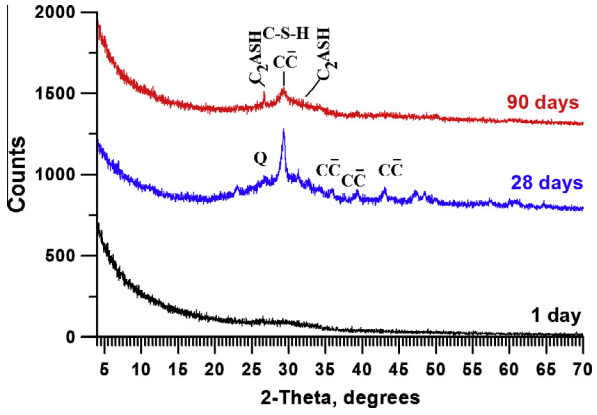

Fig. 16. XRD pattrens mix S6 activated with (1.50:0.50; Na_2O:SiO_2 mol/kg) cured up to 90 days.

3.9. Fourier transformation infrared spectroscopy

Figs. 17–19 show the FTIR spectra of alkaline activated GBFS pastes. The bands at 460–465 cm^{-1} are attributed to in plane Si—O bending and Al—O linkages [74]. The band at around 1002 cm^{-1} is due to T—O—Si (T: Si or Al) asymmetric stretching vibration (950–1200 cm^{-1}) as a result of TO_4 reorganization that takes place during synthesis [75]. The band located at 1002 cm^{-1} are a major fingerprint of the inorganic polymeric matrix and define the extent

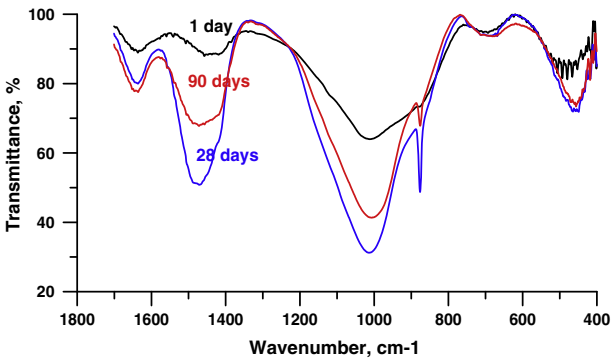

Fig. 17. FTIR of mix S1 activated with (0.25:0.50; Na_2O:SiO_2 mol/kg) cured up to 90 days.

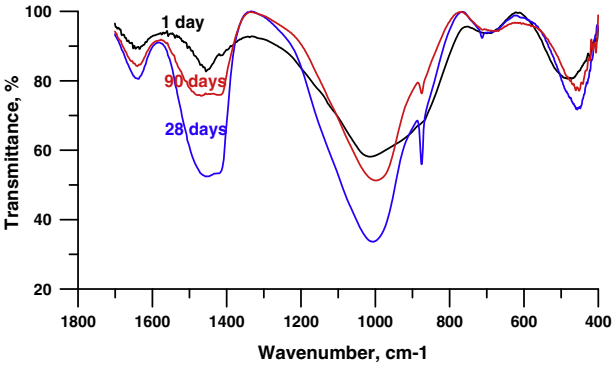

Fig. 18. FTIR of mix S3 activated with (0.75:0.50; Na_2O:SiO_2 mol/kg) cured up to 90 days.

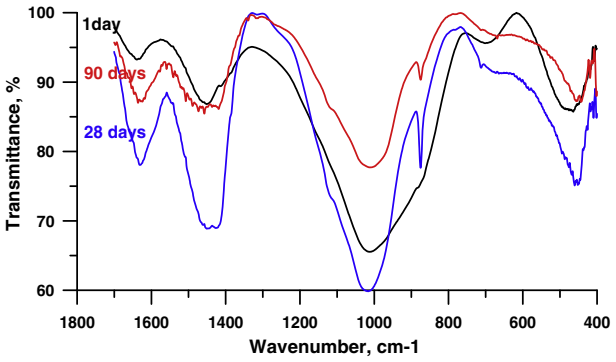

Fig. 19. FTIR of mix S6 activated with (1.50:0.50; Na_2O:SiO_2 mol/kg) cured up to 90 days.

of polysialation or aluminium incorporation [75,76]. The very strong peaks seen at ~1002 cm^{-1} (as well as at ~458 cm^{-1}) are assigned to long chain bonds and/or the excess of Al—Si gel formed [76].

The FTIR band at 1040 cm^{-1} in the initial sample progressively shifted as a function of the reaction time to 1030 cm^{-1} after 90 days (Figs. 17–19). This band was attributed to asymmetrical stretching Si—O(Si) and Si—O(Al) vibrations in external tetrahedral sites, and the shift indicates that aluminium species are inserted into the framework. Bands at 1040 cm^{-1} are assigned to stretching of Si—O—Si bonds at the surface of the unreacted silica particles [77], and bands at 1100, 800 and 475 cm^{-1} relate to stretching, bending and rocking of the Si—O—Si bonds within the network of the unreacted GBFS particles. Bands at 545, 625 and 700 cm^{-1} are also, related to vibrations in the unreacted particles of GBFS.

The main binder gel band appears at 1010 cm^{-1}, assigned to the asymmetric stretching mode of the Si—O—T (T: tetrahedral Si or Al) bonds within the reaction products. The position of this band is consistent with both the C—(A)—S—H structure formed by the activation of GBFS [66,78,79]. The band at 999–1010 cm^{-1}, it is typically associated with the binding gels (C—(A)—S—H and N—A—S—H, relatively low wavenumber can be attributed to a reduced content of calcium in the C—(A)—S—H formed from the activation of the GBFS, and increased incorporation of Al into this gel, as the availability of this element increases in the systems by the dissolution.

Atmospheric carbonation is evident at the region of 1455 and 875 cm^{-1}; part of the excess Na present in the matrix is carried to the surface where it reacts with carbon dioxide. The band at 875 cm^{-1} was not observed in the initial sample, but it was present in all the FTIR spectra of samples after the pozzolanic reaction attributed to the carbonation of samples during manipulation once the pozzolanic reaction finished. The bands are associated with pure $CaCO_3$, attributed to out-of-plane deformation and asymmetric stretching vibrations, respectively. Both bands shift to higher wave numbers after the activation process which, relates to CO_3^{2-} impurity species. This, together with the higher intensity of the peaks appearing in the spectrum of the sample activated at 28 days was observed (Figs. 17–19).

The presence of unreacted particles gives rise to a series of bands located at, 1084, 796–778, 697, 668, 522 and 460 cm^{-1} in the IR spectrum [80]. Although, these bands persist after activation, a reduction in intensity is observed, which indicates that presence of unreacted particles has partially reacted. The higher reduction observed for the sample containing 1.50:0.50; Na_2O:SiO_2 mol/kg implies greater reactivity (Fig. 19), which leads to further development of the alkali-activation reaction products. These results are consistent with the lower porosity and improved compressive strength presented by the samples alkali-activated with 1.50:0.50; Na_2O:SiO_2.

The interpretation of the wide and intense band appears from 990 cm^{-1} to 1200 cm^{-1} may be difficult, as bond vibrations of different compounds tend to overlap, producing a highly complex spectrum. While in the unreacted GBFS particles this band appears at 1015 cm^{-1}, in the activated samples it shifts to lower wavenumbers (1001 cm^{-1}). This shift occurs due to the formation of aluminosilicate gel, as the asymmetric stretching vibrations of the newly formed Si—O—T (T = Al, Si) bonds originate a new band growing at 990 cm^{-1} as shown in Figs. 18 and 19. Although a gel with a higher Si/Al ratio is expected for the 1.50:0.50; Na_2O:SiO_2 paste, the nature of the gel formed could not be clearly distinguished from FTIR results, due to the Al-enriched gel phase band (1015 cm^{-1}, from [81], and the primary band of the Si—O—T bonds in the gel overlap. Furthermore, the bands associated with the vitreous phases of the raw material were also expected to appear in this region (950–1100 cm^{-1} [80]. Although they could not be distinguished, the intensity was expected to decrease as the alumino-silicate gel formation proceeded.

After 90 days, there is a reduction the in intensity of the main Si—O—Si band, indicating that the solid silica is dissolving. At the same time, a new band starts forming at about 950 cm^{-1} and the intensity of this band increases over time. This particular band is associated with the Si—O—T stretch within the newly formed geopolymer network [76], and it appears to grow at a similar rate in both samples depicted in Figs. 17–19.

Band descriptions are as follows: bending vibration of HOH in the region of 1595–1628 cm^{-1}, stretching vibration of CO_2 located at about 1430 cm^{-1}, asymmetric stretching vibration of T—O—Si at about 990–1100 cm^{-1}, where T = Si or Al, Si—O stretching in the region of 880 cm^{-1}, symmetric stretching vibration of Si—O—Si between 770 and 780 cm^{-1}, symmetric stretching vibration of Si—O—Si and Al—O—Si in the region 675–685 cm^{-1} and bending vibration of Si—O—Si and O—Si—O in the region 450–460 cm^{-1}. The bending vibration of Si—O—Si appeared to increase in sharpness with increasing the Na_2O content from 0.25 to 1.5. The broadness of HOH band implies the overlap of more bands with higher intensity which is mainly related to the combined water in CSH, and so, the increase of this peak reflects the increase of binding materials of this specimen. This band decreases sharply with the Na_2O content from 0.25 to 1.5 at 90 days, due to in the formation of two-dimensional polysialatedisiloxo crosslink than forming CSH which in turn acts as a seeding agent for geopolymer accumulation.

In conclusion, various infrared absorption bands may be used for the identification of bonds such as Si—O, Al—O and S—OH in the inorganic polymer structure. These bonds are formed when GBFS particles react with the activating solution and solubilization of elements takes place. Stretching vibrations of the bond T—O—Si seen between 950 and 1200 cm^{-1} indicate the formation of gel during polycondensation.

3.10. Scanning electron microscopy

Figs. 20–22 show the SEM micrographs of samples S1, S3 and S6 hydrated for 3, and 90 days respectively. Fig. 20 shows SEM micrograph of S1 sample hydration at 3 days under alkaline condition (0.25:0.50; Na_2O:SiO_2 mol/kg), micrograph represented the formation of thin film of hydration products on the surface of alkaline activated GBFS paste. This initial hydration products are amorphous with a honeycomb like structure C—S—H gel with the metastable state. H_2O and OH^- permeate through the initial hydration products and reacted with GBFS particles with the increase of hydration age, to produce more hydration products. With the increase of the hydration age (90 days), the surface of active components of alkaline activated GBFS paste are corroded more obviously and hydration products can be clearly observed on the surface of alkaline activated GBFS particles. SEM micrograph deposited the hydration products on the surface of alkaline activated GBFS particles are more obvious. Most of the gel produced by alkaline activated GBFS paste hydration is the hydration products similar to the C—S—H gel as well as flake crystal of calcium aluminate hydrates.

Figs. 21 and 22 represented the SEM micrographs of S3 and S6 hydrated for 3, and 90 days respectively. The increasing of the alkalinity condition increase the promoting effect on the early hydration of alkaline activated GBFS. The gel was formed on the surface of alkali activated GBFS. The hydration products appeared as nearly amorphous C—S—H gel covering the grains of anhydrous alkali activated GBFS particles appeared in the structure (Figs. 21 and 22). Globules of C—S—H or C—A—S—H are concentrated in the matrix. The micrograph shows the flocculent and porous structures as well as wider pores are available for crystallization of the formed hydrates. Pastes cured for 90 days have a compact-dense microstructure displayed a more dense arrangement of microcrystalline C—S—H and C—A—H as the main hydration products (Figs. 21 and 22). The amount of amorphous gel is very high, occupying an important part of the volume in the sample. Furthermore, SEM images showed an important amount of (N,C)—A—S—H gel and low porosity of the developed matrix [65]. With the increase of the content of Na_2O leads to form a denser closed microstructure, leading to higher compressive strength values. Furthermore, all the pastes presented unreacted particles surrounded by hydration products.

3.11. Resistance to aggressive attack

3.11.1. Magnesium sulphate solution

The problem of aggressive attack of sulphate and chloride ions has been of considerable scientific and technological interest

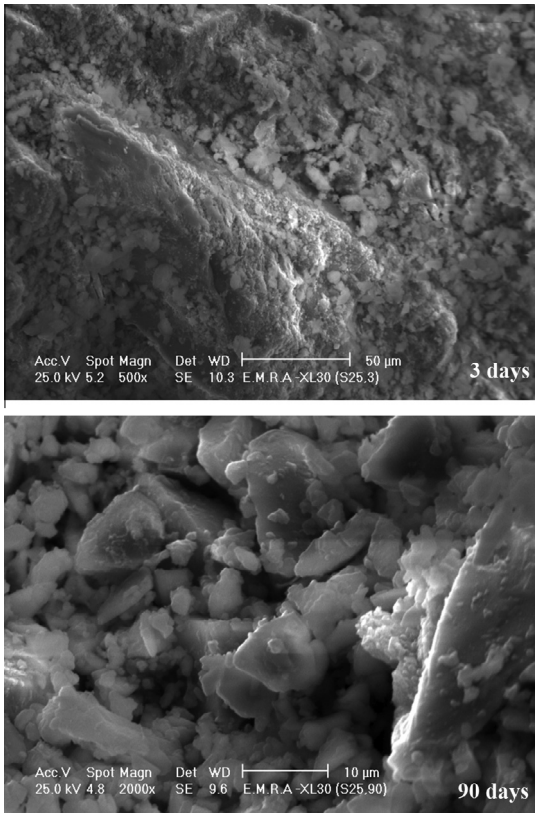

Fig. 20. SEM micrograph of mix S1 activated with (0.25:0.50; Na_2O:SiO_2 mol/kg) cured up to 3 and 90 days.

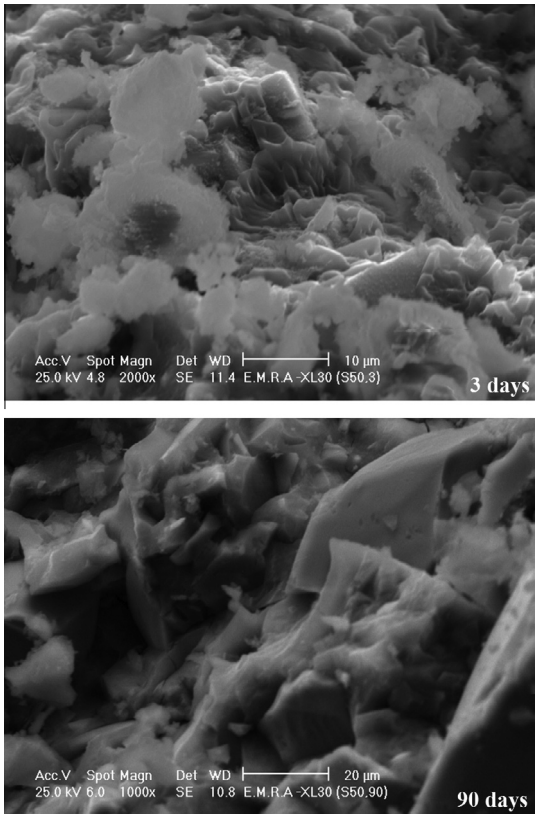

Fig. 21. SEM micrograph of mix S3 activated with (0.75:0.50; Na_2O:SiO_2 mol/kg) cured up to 3 and 90 days.

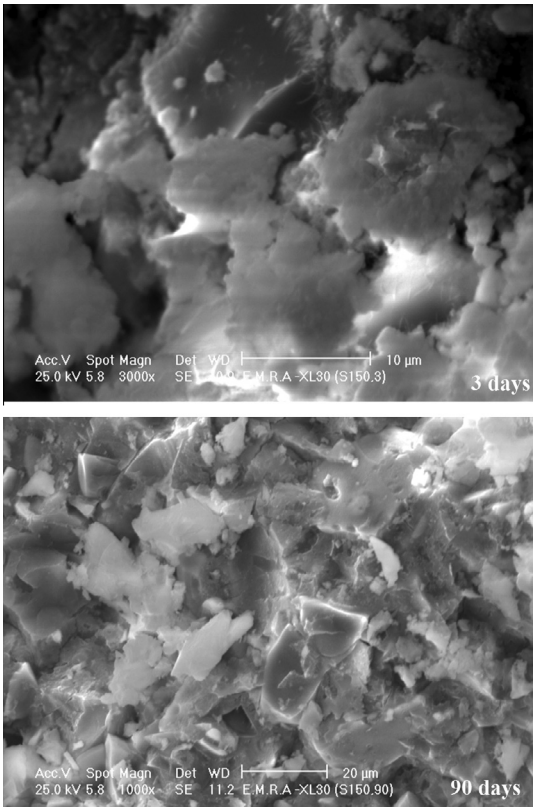

Fig. 22. SEM micrograph of mix S6 activated with (1.5:0.50; Na_2O:SiO_2 mol/kg) cured up to 3 and 90 days.

because this attack is one of the factors responsible for concrete damage. Sulphate ions can inter into chemical reactions with certain constituents of concrete producing sulphoaluminate hydrates and gypsum, which cause the expansion of concrete [35,38]. Magnesium sulphate causes distress into concrete decreasing OH^- concentration; C—S—H phase may be decomposed and caused losses in strength [82].

3.11.1.1. Compressive strength. The compressive strength of alkali activated GBFS as well as OPC immersed in 5% $MgSO_4$ solution up to 180 days is graphically plotted in Fig. 23. The data show that the compressive strength of alkaline activated slag increases with curing time as the hydration progresses up to 180 days. The compressive strength of mix S1 shows higher values, due to a good pozzolanic activity in alkaline activation that exhibits higher resistance to sulphate medium up to 180 days. The immersion of alkali activated GBFS pastes in 5% $MgSO_4$ solution enhances the activation of GBFS pastes. The high compressive strength of OPC pastes at zero time is due to its higher rate of hydration compared to alkali activated GBFS. It is clear that the compressive strength of alkali activated GBFS increases up to 180 days. Alkali activated GBFS improves the durability and the resistance to chemical attack, this is due to the continuous activation of GBFS forming C—S—H as well as C—A—S—H. The compressive strength of OPC pastes immersed in 5% $MgSO_4$ increases up to 180 days then decreases [10,35,38,42]. The decrease of strength of OPC pastes after 180 days is mainly due to the presence of high values of alite and belite, which liberate $Ca(OH)_2$ [35,38,42]. The liberated $Ca(OH)_2$ available in the hydrated cement matrix reacted with $MgSO_4$ to form gypsum. The formed gypsum reacted with calcium aluminated phases of both hydrated and the unhydrated portions of cement in the matrix to form expanding ettringite [82–85]. On the other side, the presence of magnesium ions as $MgSO_4$ or/and

$MgCl_2$ leads to the distortion of C—S—H through a dissolution of Ca^{2+} or/and an exchange with Mg^{2+} to Mg—S—H and $Mg(OH)_2$ which have no binding properties [35,38]. By comparing the alkali activated slag with OPC, it is found that the strength of alkali activated slag increases up to 180 days, due to the formation of additionally C—S—H [70], without the formation of expanding and softening chloroaluminate and ettringite hydrated products.

3.11.1.2. Total sulphate content. The total sulphate content of alkali activated GBFS as well as OPC immersed in 5% $MgSO_4$ solution up to 180 days is graphically represented in Fig. 24. The data show that the total sulphate contents of alkali activated GBFS has the lower values of sulphate content up to 180 days of immersion in 5% $MgSO_4$ solution. The resistance towards sulphate attack solution increases with the increase of alkali activated contents. This is mainly due to the decrease of the total porosity which hinders the penetration of sulphate ions in the matrix. The values of total sulphate contents increase with the immersing time due to immersion of pastes in aggressive medium containing sulphate ions (5% $MgSO_4$). OPC pastes give higher values of total sulphate content than those alkali activated GBFS. S5 has a lower values of total sulphate content up to 180 days, this can be attributed to the fact that the alkali activated GBFS do not have free lime content in its matrix and geopolymers themselves are not easily attacked by aggressive medium containing sulphate ions as shown in Fig. 24 [46].

3.11.2. Magnesium chloride solution

The corrosive action of chlorides is due to the formation of chloroaluminate hydrates, which causes softening of concrete. Attack of chlorides proceeds by ionic penetration of Cl^- in concrete. This penetration is independent of the chloride concentration and the concrete penetrability to the salt solution as a whole. Diffusion seems to be dependent not only on the porosity of the matrix but also on the nature of the paste. Moreover, Cl^- ionic diffusion depends not only on the permeability and binding capacity of Cl^- ions, but also on the ion-exchange capacity of the system.

3.11.2.1. Compressive strength. The compressive strength values of hydrated alkali activated GBFS pastes immersed in 5% $MgCl_2$ solution up to 180 days are graphically represented in Fig. 25. The compressive strength increases with curing time, due to the continuous hydration. The compressive strength of mix S1 shows a sharp increase up to 28 days, and then it increases slowly up to 180 days. The compressive strength of mix S5 increases gradually up to 180 days due to good resistance to chloride medium, whereas, the values of compressive strength of OPC shows a lower values

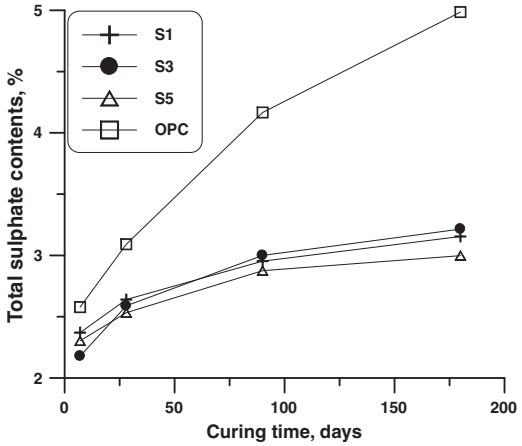

Fig. 24. Total sulphate of hardened cement pastes subjected to 5% $MgSO_4$ solution up to 180 days.

from 28 days up to 180 days. OPC contains free lime content in its matrix due to hydration reactions of Portland cement portion, this free lime and also the hydrated Portland cement matrix C—S—H gel of the matrix are easily attacked by acids in general [42,82].

3.11.2.2. Total chloride content. The total chloride contents of alkali activated GBFS pastes immersed in 5% $MgCl_2$ solution up to 180 days is graphically plotted in Fig. 26. The total chloride content increases with curing time for all mixes up to 180 days. The total chloride sharply increases after 1 week, then slowly increases up to 180 days for all pastes. The total chloride content decreases with alkali dosages due to the pozzolanic reaction to form C—S—H that fill some available open pores, thereby inhibiting the chloride ion penetration; improve the microstructure of pore systems. The increase in total chloride contents of OPC paste is mainly is due to the reaction of $MgCl_2$ with CH forming $CaCl_2$ and $Mg(OH)_2$. $CaCl_2$ reacts with C_3A and/or C_4AF to form chloroaluminate hydrate ($C_3A{\cdot}CaCl_2{\cdot}10H_2O$). Also, $MgCl_2$ reacts with calcium silicate hydrates form calcium chloride, magnesium hydroxide and silica gel. The alkali activated GBFS do not have free lime content in its matrix and geopolymers themselves are not easily attacked by aggressive medium containing [46]. These is mainly due to the accumulation of excessive amounts of hydrates within the pore systems at larger hydration times; this effect leads to a decreased accessibility of chloride ions towards the more dense with low capillary pore structure of the hardened pastes on the prolonged hydration.

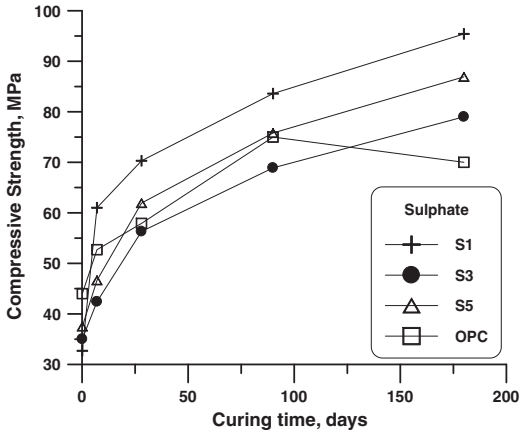

Fig. 23. Compressive strength of activated GBFS subjected to 5% $MgSO_4$ solution up to 180 days.

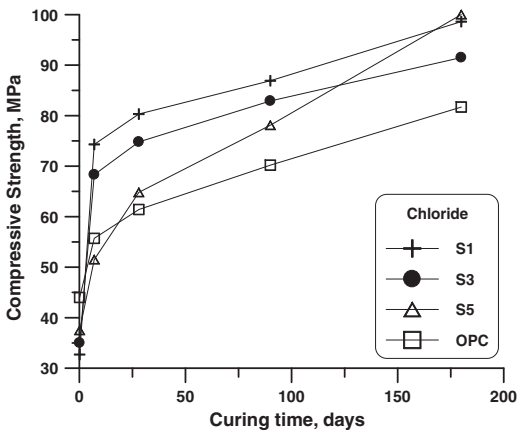

Fig. 25. Compressive strength of activated GBFS subjected to 5% $MgCl_2$ solution up to 180 days.

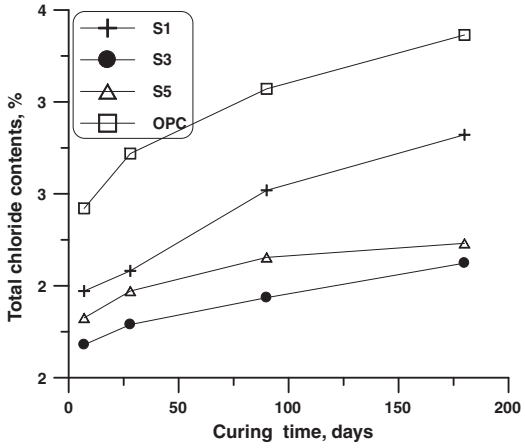

Fig. 26. Total chloride of hardened cement pastes subjected to 5% $MgCl_2$ solution up to 180 days.

4. Conclusions

The main conclusions could be derived from this investigation are summarized as follows:

1. Electrical conductivity of alkali activated GBFS depends mainly on the binder composition, the activator type and its concentration. Alkali activator contents affected the location and intensities of the conductivity maximum.
2. Mix S5 shows the higher values of compressive strength at all curing ages up to 90 days.
3. The improvement on compressive strength is related to the reorganization in the microstructure of alkali activated GBFS system.
4. The compressive strength of mix S1 shows higher values in 5% $MgSO_4$ or $MgCl_2$ up to 180 days, due to a good pozzolanic activity in alkaline activation that exhibits higher resistance to sulphate medium up to 180 days.
5. Alkali activated GBFS lead to good durability and high resistance to chemical attack.
6. By comparing the alkali activated slag with OPC, it is found that the strength of alkali activated slag increases up to 180 days, due to the formation of C—S—H and geopolymer with the absence of chloroaluminate and ettringite.
7. Total sulphate of mix S5 have a lower value up to 180 days.
8. The total chloride and total sulphate contents decrease with alkali activated GBFS due to the forming hydrated products that fill some available open pores, thereby inhibiting Cl^- and SO_4^{2-} ions penetration; this effect leads to a decreased accessibility of Cl^- or SO_4^{2-} ions towards the more dense with low capillary pore structure of the hardened pastes on the prolonged hydration.
9. It can be concluded that alkali activated GBFS are more durable in 5% $MgSO_4$ or 5% $MgCl_2$ than OPC pastes.

References

[1] Shi C, Krivenko PV, Roy DM. Alkali-activated cements and concretes. Abingdon (UK): Taylor & Francis; 2006.
[2] Talling B, Krivenko PV. Blast furnace slag – the ultimate binder. In: Chandra S, editor. Waste materials used in concrete manufacturing. Park Ridge (NJ): Noyes Publications; 1997. p. 235–89.
[3] USEPA. Wastes-resource conservation-reduce, reuse, recycle-construction & demolition materials; 2009. <http://www.epa.gov/epawaste/conserve/rrr/imr/cdm/index.htm>.
[4] Gartner E. Industrially interesting approaches to "low-CO_2" cements. Cem Concr Res 2004;34(9):1489–98.
[5] Malhotra VM. In: Gjorv OE, Sakai K, editors. Concrete technology for a sustainable development in the 21st century. London: E & FN Spon; 2000. p. 226.
[6] McCaffrey R. Climate change and the cement industry. Glob Cem Lime Mag (environmental special issue); 2002. p. 15.
[7] Provis JL. Activating solution chemistry for geopolymers. In: Provis JL, van Deventer JSJ, editors. Geopolymers: structures, processing, properties and industrial applications. Abingdon: Woodhead Publishing; 2009. p. 50–71.
[8] Van Deventer JSJ, Provis JL, Duxson P, Brice DG. Chemical research and climate change as drivers in the commercial adoption of alkali-activated materials. Waste Biomass Valoriz 2010;1(1):145–55.
[9] Herr R. Die Entwicklung von Baustoffen nach dem Prinzip der Geopolymerization, IEMB, Neue Ergebnise; 2002. 6 ps What is geopolymer? <www.geopolymer.org/about3.html>.
[10] Duxson P, Fernandez-Jimenez A, Provis JL, Lukey GC, Palomo A, Van Deventer JSJ. Geopolymer technology: the current state of the art. J Mater Sci 2007;42:2917–33.
[11] Li Z, Ding Z, Zhang Y. Development of sustainable cementitious materials. In: Proceedings of international workshop on sustainable development and concrete technology, Beijing, China; 2004. p. 55–76.
[12] Drechsler M, Graham A. Innovative material technologies: bringing resources sustainability to construction and mining industries. In: Shi C, Fernandez-Jimenez AJ. 48th Institute of quarrying conference, Adelaide. Hazard Mater B1 2006; 37: 1656–63.
[13] Majidi B. Geopolymer technology, from fundamentals to advanced applications: a review. Mater Technol 2009;24(2):79–87.
[14] Detphan S, Chindaprasirt P. In: Technology and innovation for sustainable development conference (TISD2008); 2008. p. 111.
[15] Collins FG, Sanjayan JG. Workability and mechanical properties of alkali-activated slag concrete. Cem Concr Res 1999;29(3):455–8.
[16] Collins FG, Sanjayan JG. Effect of ultra fine materials on workability and strength of concrete containing alkali-activated slag as the binder. Cem Concr Res 1999;29(2):459–62.
[17] Collins FG, Sanjayan JG. Strength and shrinkage properties of alkali-activated slag concrete containing porous coarse aggregate. Cem Concr Res 1999;29(4):607–10.
[18] Collins FG, Sanjayan JG. Strength and shrinkage properties of alkali-activated slag concrete placed into a large column. Cem Concr Res 1999;29(5):659–66.
[19] Collins FG, Sanjayan JG. Cracking tendency of alkali-activated slag concrete subjected to restrained shrinkage. Cem Concr Res 2000;30(5):791–8.
[20] Collins FG, Sanjayan JG. Effect of pore size distribution on drying shrinkage of alkali-activated slag concrete. Cem Concr Res 2000;30(9):1401–6.
[21] Collins FG, Sanjayan JG. Early age strength and workability of slag pastes activated by sodium silicates. Mag Concr Res 2001;52(5):321–6.
[22] Guerrieri M, Sanjayan J, Collins F. Residual strength properties of sodium silicate alkali activated slag paste exposed to elevated temperatures. Mater Constr 2010;43(6):765–73.
[23] Fernandez-Jimenez A, Puertas F. Effect of activator mix on the hydration and strength behavior of alkali-activated slag cements. Adv Ceram Res 2003;15:129–36.
[24] Ben Hafa M, Le Saout G, Winnefeld F, Lothenbach B. Influence of activator type on hydration kinetics, hydrate assemblage and microstructural development of alkali-activated blast-furnace slags. Cem Concr Res 2011;41:301–10.
[25] Rodriguez E, Bernal S, Mejiade Guterrez R, Puertas YF. Alternative concrete based on alkali-activated slag. Mater Constr 2008;58:53–67.
[26] Palacios M, Puertas YF. Effect of superplasticizer and shrinkage-reducing admixtures on alkali-activated slag pastes and mortars. Cem Concr Res 2005;35:1358–67.
[27] Purdon AO. The action of alkalis on blast-furnace slag. J Chem Ind 1940;59:191–202.
[28] Glukhovsky VD, Rostovkaya GS, Rumyna GV. High strength slag-alkali cement. In: 7th Intern congr chem cem, Paris, France; 1980, III, V. p. 164–8.
[29] Wang S-D, Scrivener KL, Pratt PL. Factors affecting the strength of alkali-activated slag. Cem Concr Res 1994;24:1033.
[30] Douglas E, Brandstetr J. A preliminary study on the alkali activation of granulated blast furnace slag. Cem Concr Res 1990;20(5):746–56.
[31] Shi C, Day RL. Some factors affecting early hydration of alkali-slag cements. Cem Concr Res 1996;26:439–77.
[32] Slota RJ. Utilization of water glass as an activator in the manufacturing of cementitious materials from waste by-products. Cem Concr Res 1987;17:703–8.
[33] Fernández-Jiménez A, Palomo A. Composition and microstructure of alkali activated fly ash binder: effect of the activator. Cem Concr Res 2005;35(10):1984–92.
[34] Abd El Aziz M, Abd El Aleem S, Heikal M, El Didamony H. Hydration and durability of sulphate-resisting and slag cement blends in Caron's Lake water. Cem Concr Res 2005;35:1592–600.
[35] Ghosh SN, Sarkar SL, Harsh S. Progress in cement and concrete, mineral admixtures in cement and concrete. In: Moukwa M, editor. Durability of silica fume concrete, vol. 4. New Delhi: ABI Books; 1993. p. 467–93.
[36] Amin AM, Ali AH, El-Didamony H. Durability of some Portland cement pastes in various chloride solutions. Zem-Kalk-Gips 1997;50(3):172–7.
[37] Abd-El-Eziz MA, Heikal M. Hydration characteristics and durability of cements containing fly ash and limestone subjected to Qaron's Lake water. Adv Cem Res 2009;21(3):91–9.

[38] El-Didamony H, Heikal M, Al-Masry S. Effect of delaying addition time of SMF superplasticizer on the physic-mechanical properties and durability of cement pastes. Constr Build Mater 2012;35:261–9.
[39] Aiad I, El-Didamony H, Heikal M, Al-Masry S. Effect of delaying addition time of synthesized SSPF condensate on the durability of sulphate resisting cement pastes incorporating micro-silica. Constr Build Mater 2013;48:1092–103.
[40] El-Didamony H, Aiad I, Heikal M, Al-Masry S. Impact of delayed addition time of SNF condensate on the fire resistance and durability of SRC–SF composite cement pastes. Constr Build Mater 2014;50:281–90.
[41] El-Didamony H, Amer AA, Abd Ela-ziz H. Properties and durability of alkali-activated slag pastes immersed in sea water. Ceram Int 2012;38:3773–80.
[42] Bernal SA, Mejia de Gutierrez R, Pedraza AL, Provis J. Effect of binder content on the performance of alkali-activated slag concretes. Cem Concr Res 2011;41:1–8.
[43] Bakharev T, Sanjayan JG, Cheng YB. Sulfate attack on alkali-activated slag concrete. Cem Concr Res 2002;32:211–6.
[44] Puertas F, Mejia de Gutierrez R, Fernandez-Jimenez A, Delvasto S, Maldonado J. Alkaline cement mortars, chemical resistance to sulphate and seawater attack. Mater Constr 2002;52(267):55–71.
[45] Bakharev T, Sanjayan JG, Cheng YB. Resistance of alkali-activated slag concrete to acid attack. Cem Concr Res 2003;33:1607–11.
[46] Escalante-Garcia JI, Fuentes AF, Gorokovsky A, Fraire-Luna PE, Mendoza-Suarez G. Hydration products and reactivity of blast-furnace slag activated by various alkalis. J Am Ceram Soc 2003;86(12):2148–53.
[47] Fernandez-Jimenez A, Puertas F, Sorbrados I, Sanz J. Structure of calcium silicate hydrates formed in alkaline activated slag. Influence of the type of alkaline activator. J Am Ceram Soc 2003;86(8):1389–94.
[48] Puertas F, Fernandez-Jimenez A, Blanco-Varela MT. Pore solution in alkali-activated slag cement pastes. Relation to the composition and structure of calcium silicate hydrate. Cem Concr Res 2004;34:139–48.
[49] Darko K, Branislav Z. Effects of dosage and modulus of water glass on early hydration of alkali-slag cements. Cem Concr Res 2002;32:1181–8.
[50] Atis Cengiz D, Bilim C, Özlem C, elik Okan K. Influence of activator on the strength and drying shrinkage of alkali-activated slag mortar. Constr Build Mater 2009;23:548–55.
[51] Wang SD, Scrivener KL. ^{29}Si and ^{27}Al NMR study of alkali-activated slag. Cem Concr Res 2003;33:769–74.
[52] Glukhovsky V. Ancient, modern and future, concretes. In: Krivenko PV, editor. Proceedings of the first international conference on alkaline cements and concretes, Kiev, Ukraine, VIPOL Stock Company, vol. 1; 1994. p. 1–8.
[53] Krivenko PD. Alkaline cements. In: Paper presented at the first international conference on alkaline cement and concretes, Kiev, Ukraine; 1994.
[54] Fernandez-Jimenez A, Puertas F. Setting of alkali-activated slag cement. Influence of activator nature. Adv Cem Res 2001;13(3):115–21.
[55] Wang SD, Pu XC. The role of different anions and cations of alkali component in the process of hydration of alkali-slag blend. In: Proceedings of the 4th international conference on fly ash, silica fume, slag and natural pozzolans in concrete, Istanbul, Turkey, vol. 2; 1992. p. 803–10.
[56] American Society for Testing and Materials American Society for Testing and Materials. ASTM standards, standard test method for normal consistency of hydraulic cement, American Society for Testing and Materials, C 187-83; 2008. p. 195.
[57] Heikal M, Aiad I, Helmy IM. Portland cement clinker, granulated slag and by-pass cement dust composites. Cem Concr Res 2002;32:1805–12.
[58] Heikal M, Morsy MS, Radwan MM. Electrical conductivity and phase composition of calcium aluminate cement containing air-cooled and water cooled slag at 20, 40 and 60 °C. Cem Concr Res 2005;35(7):1438–46.
[59] Heikal M, Morsy MS, El-Shimy E, Abo-El-Enein SA. Hydrothermal reactivity of granulated slag and sand using a lime-rich industrial waste as an activator. l'industria italiana del Cemento (iiC) 2004(7–8):614–25.
[60] Stark J, Ludwing HM, Müller A. Determination of the degree of hydration of slag cements. ZKG 1991;90(11):557–60.
[61] Heikal M, Radwan MM. Physico-chemical properties and microstructure of some blended systems. Sil Ind 2006;71(9–10):161–6.
[62] Heikal M, Radwan MM, Morsy MS. Influence of curing temperature on the physico-mechanical, characteristics of calcium aluminate cement with air-cooled slag or water-cooled slag. Ceram Silik 2004;48(4):185–96.
[63] Criado M, Fernandez-Jimenez A, de la Torre AG, Aranda MAG, Palomo A. An XRD study of the effect of the SiO_2/Na_2O ratio on the alkali activation of fly ash. Cem Concr Res 2007;37(5):671–9.
[64] Shi C. Early hydration and microstructure development of alkali-activated slag pastes. In: 10th International congress on the chemistry of cement, Gothenburg, Sweden, vol. 3ii099; 1997. p. 8.
[65] Tashima MM, Soriano L, Borrachero MV, Monzó J, Payá J. Effect of curing time on microstructure and mechanical strength development of alkali activated binders based on vitreous calcium aluminosilicate (VCAS). Bull Mater Sci 2013;36(2):245–9.
[66] Aydın S, Baradan B. Effect of activator type and content on properties of alkali-activated slag mortars. Composites: Part B 2014;57:166–72.
[67] Silva PDe, Sagoe-Crenstil K, Sirivivatnanon V. Kinetics of geopolymerization: Role of Al_2O_3 and SiO_2. Cem Concr Res 2007;37(4):512–8.
[68] Wang KS, Lin KL, Huang ZQ. Hydraulic activity of municipal solid waste incinerator fly-ash-slag-blended eco-cement. Cem Concr Res 2001;31:97–103.
[69] Jiaying S, Peinan Z. Liquor into the hydration mechanism of the blast-furnace slag in the alkali solution. Bull Chin Ceram Soc 1988;7(6):16–24.
[70] Yip Christina K, Lukey Grant C, Provis John L, Van Deventer Jannie SJ. Effect of calcium silicate sources on geopolymerzation. Cem Concr Res 2008;38:554–64.
[71] Tashima MM, Akasaki JL, Castaldelli VN, Soriano L, Monzó J, Payá J. New geopolymeric binder based on fluid catalytic cracking catalyst residue (FCC). Mater Lett 2012;80:50–2.
[72] Ramachandran VS, Paroli RM, Beaudoin JJ, Degado AH. Handbook of thermo-analysis of construction materials. Noyes: William Andrew Publishing; 2002.
[73] Yip CK, Van Deventer JSJ. Microanalysis of calcium silicate hydrate gel formed within a geopolymeric binder. J Mater Sci 2003;38(18):3851–60.
[74] Van Jaarsveld JGS, Van Deventer JSJ, Lukey GC. The effect of composition and temperature on the properties of fly ash- and kaolinite-based geopolymers. J Chem Eng 2002;89:63–73.
[75] Gadsden A. Infrared spectra of minerals and related inorganic compounds. London: Butterworths; 1975.
[76] Rees CA, Provis JL, Lukey GC, van Deventer JSJ. Attenuated total reflectance Fourier transform infrared analysis of fly ash geopolymer gel ageing. Langmuir 2007;23:8170–9.
[77] Lloyd RR, Provis JL, van Deventer JSJ. Microscopy and microanalysis of inorganic polymer cements. 2: The gel binder. J Mater Sci 2009;44(2):620–31.
[78] Garcia-Lodeiro I, Palomo A, Fernéndez-Jiménez A, Mac-Phee DE. Compatibility studies between N—A—S—H and C—A—S—H gels. Study in the ternary diagram Na_2O—CaO—Al_2O_3—SiO_2—H_2O. Cem Concr Res 2011;41(9):923–31.
[79] Puertas F, Palacios M, Manzano H, Dolado JS, Rico A, Rodríguez J. A model for the C—A—S—H gel formed in alkali-activated slag cements. J Eur Ceram Soc 2011;31(12):2043–56.
[80] Criado M, Fernández-Jiménez A, Palomo A. Alkali activation of fly ash: effect of the SiO_2/Na_2O ratio Part I: FTIR study. Micropor Mesopor Mater 2007;106:180–91.
[81] Hajimohammadi A, Provis JL, van Deventer JSJ. Time-resolved and spatially-resolved infrared spectroscopic observation of seeded nucleation controlling geopolymer gel formation. J Colloid Interface Sci 2011;357:384–92.
[82] Hime WG, Mather B. Sulphate attack or is it? Cem Concr Res 1999;29:789–91.
[83] Hewlett PC. Lea's chemistry of cement and concrete. Butterworth-Heinemann, Technology & Engineering; 2003. p. 1092.
[84] Dinakar P, Babu KG, Santhanam M. Durability properties of high volume fly ash self compacting concretes. Cem Concr Compos 2008;30(10):880–6.
[85] Rajamane NP, Nataraja MC, Lakshmanan N, Dattatreya JK, Sabitha D. Sulphuric acid resistant ecofriendly concrete from geopolymerisation of blast furnace slag. Indian J Eng Mater Sci 2012;19(5):357–67.